JOURNAL OF SOLID STATE CHEMISTRY **124,** 250–263 (1996)
ARTICLE NO. 0234

Magnetic and Electrical Properties of $La_yA_xMn_wO_3$ (A = Na, K, Rb, and Sr) with Perovskite-Type Structure

Tetsuo Shimura, Toshimasa Hayashi, Yoshiyuki Inaguma, and Mitsuru Itoh

Research Laboratory of Engineering Materials, Tokyo Institute of Technology, 4259 Nagatsuta-cho, Midori-ku, Yokohama 226 Japan

Received August 16, 1995; in revised form April 3, 1996; accepted April 10, 1996

Substitution of Na, K, Rb, and Sr for La in the perovskite type structure complex oxide $LaMnO_3$ were carried out and their structure and properties were investigated. Lattice symmetry of the samples sintered at 1393 K in O_2 gas flow was found to be rhombohedral. Rietveld refinement to X-ray diffraction data revealed a systematic decrease of the lattice distortion with substitution. The change of temperature dependence of resistivity from semiconducting to metallic and the increase of the ferromagnetic transition temperature with substitution were recognized and found to be closely related to structural changes. The anomalies in the Seebeck coefficient at the ferromagnetic transition temperature suggest a strong correlation between the electronic state and magnetism.

INTRODUCTION

Electric and magnetic properties of oxides of the perovskite type structure have been the important subject in solid state physics and chemistry. Among them, the properties of the Mn containing perovskite type oxide $LaMnO_3$ have gathered great interest because of its unique properties. Stoichiometric $LaMnO_{3.00}$ shows antiferromagnetism and semiconducting behavior. Alkali-earth metal or Pb substitutions for La induces ferromagnetism and metallic conduction. This ferromagnetic transition was first reported by Jonker and VanSanten (1, 2). Ferromagnetism and metallic conduction appeared when the degree of substitution of alkali-earth element for La was between about 15 and 50%. Zener (3) proposed the mechanism of this transition on double exchange interaction. The origin of the ferromagnetism is due to the ordering of spin moment $S = 3/2$ in the $3d\varepsilon$ orbital of Mn via transfer of the $3d\gamma$ electrons through the $2p\sigma$ orbital of the oxygen ion located at the center of two Mn ions in the perovskite type structure.

After the discovery of the ferromagnetism and metallic conduction in $La_{1-x}A_xMnO_3$ (A = Ca, Sr, Ba, and Pb) a large number of studies about these materials have been carried out. Verelst *et al.* (4) showed that the valence state of Mn could be controlled by oxygen nonstoichiometry instead of alkali-earth metal substitution for La. $LaMnO_{3+\delta}$ also shows metallic conductivity at low temperature, and the metal–semiconductor transition temperature increases with δ. Recently, a negative giant magnetic resistance (GMR) was discovered in $La_{1-x}A_xMnO_3$ (A = Ca, Sr, and Ba) (5–7): in bulk $La_{1-x}Sr_xMnO_3$, a reduction of resistance of more than three orders in magnitude is reported.

In this report, electrical and magnetic properties of the alkali metal substituted $LaMnO_3$ are reported. Since the valence state of the alkali metal ions is +1, being half of +2 for the alkali-earth metal ion, substitution with alkali metal can induce twice the increase in valence state of Mn as compared to the alkali-earth substitution. This approach can provide helpful information about the role of the valence of Mn and also about the role of structural change with substitution and about the appearance and strength of the double exchange interaction between Mn^{3+} and Mn^{4+}. Sr substitution was also carried out for comparison.

EXPERIMENTAL PROCEDURE

$La_yA_xMn_wO_3$ samples were prepared by a conventional solid state reaction method. Starting materials were La_2O_3, Na_2CO_3, K_2CO_3, Rb_2CO_3, $SrCO_3$, MnO_2, and $MnCO_3 \cdot zH_2O$. z was determined from the weight loss after thermal treatment of $MnCO_3 \cdot zH_2O$. Stoichiometric amounts of starting materials were mixed in an agate mortar with ethanol for A = Na and Sr. For A = K the stoichiometric amount of the materials were mixed in an agate mortar without ethanol. For A = Rb about 50% excess Rb_2CO_3 in weight was added to the stoichiometric amount and was mixed without ethanol. The starting material for Mn was MnO_2 for A = Na, K, and Sr. $MnCO_3 \cdot zH_2O$ was used for A = Rb. The mixed powders were calcined at 1273 K for 12 h in air. Furnace cooled powders were reground and mixed again with ethanol in an agate mortar and pressed into a pellet shape with a diameter of 10 mm and thickness of 2 mm. The pellets were sintered at 1393 K for 12–60 h in an oxygen gas flow then furnace-cooled to room temperature or quenched into liquid nitrogen.

The phase characterization and determination of lattice

0022-4596/96 $18.00

parameters were performed with powder X-ray diffraction analysis using a Mac Science MPX^{18}HF X-ray diffractometer. Rietveld refinement (8) to powder diffraction data were carried out for some samples.

The estimation of cations in the samples was carried out by ICP analysis except for the samples containing Rb. The amount of Rb was determined by atomic absorption spectroscopy analysis. The valence state of Mn was determined by the redox titration.

Electrical resistivities of $La_yA_xMn_wO_3$ were measured by the dc four probe method between 10 and 300 K. Magnetic susceptibilites were measured with a Quantum Design MPMS-2 SQUID magnetometer or a Shimazu MB-2 Magnetic Balance below 700 K. Seebeck coefficients were measured between 80 K and room temperature.

RESULTS AND DISCUSSION

Structure Analysis

Single phase samples were obtained for the starting composition $LaMnO_3$, $La_{1-x}Na_xMnO_3$ (x = 0.05, 0.10, 0.15, and 0.20), $La_{1-x}K_xMnO_3$ (x = 0.10 and 0.20), and $La_{0.90}Rb_{0.10}MnO_3$. Although 20% substitution of Rb for La was reported before (9), in this study single phase samples were obtained when the degree of substitution with Rb exceeds 10%. Three Sr substituted samples were prepared. The starting compositions were $La_{0.90}Sr_{0.10}MnO_3$, $La_{0.80}Sr_{0.20}MnO_3$, and $La_{0.70}Sr_{0.30}MnO_3$. The lattice symmetry of all the samples sintered at 1393 K in O_2 gas flow was found to be rhombohedral. This sintering temperature 1393 K is the lowest temperature at which the single phase sample of $La_{0.95}Na_{0.05}MnO_3$ (initial composition) was obtained. Detailed structural information about the $LaMnO_{3+\delta}$ rhombohedral phase determined from powder neutron diffraction analysis was reported by Tofield and Scott (10) and Roosmalen *et al.* (11). According to these reports, excess oxygen δ in the formula is not present as interstitial oxygen in the rhombohedral $LaMnO_{3+\delta}$ structure. So, the accurate formula taking into account the cationic defect, must be written as $(LaMn)_{1-x}O_3$. In this study, the formula $(La_{1-x}A_xMn)_{1-\delta}O_3$ was used along with previous reports. In particular, the vaporization of alkali metal and Mn during sintering cannot be neglected, so that the sum of La and alkali metal determined by ICP analysis is not equal to the amount of Mn in most samples. Taking into account these problems, the formula of sintered samples should be expressed as $La_yA_xMn_wO_3$.

Table 1 shows the accurate compositions and valence state of Mn in $La_yA_xMn_wO_3$ determined by ICP analysis and redox titration. Vaporization loss of alkali metal and Mn is apparent especially for the K and Rb systems. Only in the case of $La_{0.82}K_{0.14}Mn_{1.02}O_3$, $La_{0.84}K_{0.14}MnO_{2.98}$ is an accurate formula, because the oxygen deficiency can be more easily formed than interstitial Mn. However, the amount of alkali metal determined by analysis increases with the initial amount of alkali metal. On the other hand, the ratio x/y for Sr substitution is almost identical with the initial value.

TABLE 1
Composition and Valence State of Mn in $La_yA_xMn_wO_3$

Compositions	Average valence of Mn
$La_{0.95(1)}Mn_{0.93(1)}O_3$	3.36(3)
$La_{0.93(1)}Na_{0.04(1)}Mn_{0.96(1)}O_3$	3.31(3)
$La_{0.88(1)}Na_{0.09(1)}Mn_{0.96(2)}O_3$	3.40(3)
$La_{0.84(1)}Na_{0.12(1)}Mn_{0.97(1)}O_3$	3.45(3)
$La_{0.82(1)}Na_{0.16(1)}Mn_{1.00(1)}O_3$	3.38(3)
$La_{0.87(1)}K_{0.06(1)}Mn_{0.97(1)}O_3$	3.40(3)
$La_{0.82(1)}K_{0.14(1)}Mn_{1.02(1)}O_3$	3.33(3)
$La_{0.91(1)}Rb_{0.06(1)}Mn_{0.94(1)}O_3$	3.41(3)
$La_{0.86(1)}Sr_{0.09(1)}Mn_{0.95(1)}O_3$	3.42(3)
$La_{0.78(1)}Sr_{0.18(1)}Mn_{0.97(2)}O_3$	3.37(3)
$La_{0.70(1)}Na_{0.28(1)}Mn_{0.99(1)}O_3$	3.37(3)
$La_{0.90(1)}Na_{0.09(1)}Mn_{0.97(2)}O_3$[a]	3.29(2)
$La_{0.90(1)}K_{0.06(1)}Mn_{0.99(1)}O_3$[a]	3.26(2)
$La_{0.94(1)}Rb_{0.06(1)}Mn_{0.96(2)}O_3$[a]	3.24(2)

[a] Quenched sample.

Apparently, there is no systematic increase in the valence of Mn with y. The valence state of Mn takes values between 3.31 and 3.45, independent of x, in the furnace cooled samples. $La_{0.90}Na_{0.09}Mn_{0.97}O_3$, $La_{0.90}K_{0.06}Mn_{0.99}O_3$, and $La_{0.94}Rb_{0.06}Mn_{0.96}O_3$ are quenched samples with initial composition $La_{0.90}A_{0.10}MnO_3$. In three quenched samples the valence of manganese ion takes only slightly smaller values, between 3.24 and 3.29. The decrease of positive charge at the (La, A) site with substitution is reflected not by an increase of the valence state of Mn but by an increase of w. A similar result was reported before by Takeda *et al.* for the $La_{1-y}MnO_{3-\delta}$ system (12). In that case, the valence state of Mn is affected only by the sintering temperature.

Table 2 shows the lattice parameters and unit cell volume of $La_yA_xMn_wO_3$. For rhombohedral $LaMnO_{3+\delta}$ the space group $R\bar{3}c$ was deduced from powder neutron diffraction studies (10, 11). Values of a_h, c_h, and V_h express the lattice parameters and unit cell volume in the hexagonal $R\bar{3}c$ space group and a_r and α express the lattice parameter and angle in the rhombohedral $R\bar{3}c$ space group. The unit cell volume in the rhombohedral setting is equal to $V_h/3$. The most remarkable change with substitution appears in α, which approaches 60.0° with an increase in x. It decreases rapidly with Rb substitution, although the solubility limit for Rb substitution is smaller than for other alkali metals.

TABLE 2
Lattice Parameters and Unit Cell Volume of $La_yA_xMn_wO_3$

Composition	$a_{hex.}$ (nm)	$c_{hex.}$ (nm)	$V_{hex.}$ (nm)	$a_{rhomb.}$ (nm)	α(degree)
$La_{0.95}Mn_{0.93}O_3$	0.55265(1)	1.33345(2)	0.35279(2)	0.54716(3)	60.667(3)
$La_{0.93}Na_{0.04}Mn_{0.96}O_3$	0.55238(3)	1.33398(8)	0.35250(2)	0.54720(9)	60.627(6)
$La_{0.88}Na_{0.09}Mn_{0.96}O_3$	0.55142(1)	1.33347(1)	0.35164(2)	0.54674(2)	60.566(1)
$La_{0.84}Na_{0.12}Mn_{0.97}O_3$	0.55108(4)	1.3335(1)	0.35078(8)	0.5466(1)	60.54(1)
$La_{0.82}Na_{0.16}Mn_{1.00}O_3$	0.54903(1)	1.33186(2)	0.34830(2)	0.54550(3)	60.428(1)
$La_{0.87}K_{0.06}Mn_{0.97}O_3$	0.55235(3)	1.33642(6)	0.35311(5)	0.54785(8)	60.544(4)
$La_{0.82}K_{0.14}Mn_{1.02}O_3$	0.55055(4)	1.3377(1)	0.35116(9)	0.5479(1)	60.36(1)
$La_{0.91}Rb_{0.06}Mn_{0.94}O_3$	0.55271(2)	1.33381(2)	0.35325(6)	0.54893(3)	60.529(4)
$La_{0.86}Sr_{0.09}Mn_{0.95}O_3$	0.55242(1)	1.33481(1)	0.35312(2)	0.54738(1)	60.613(2)
$La_{0.78}Sr_{0.18}Mn_{0.97}O_3$	0.55172(1)	1.33592(2)	0.35217(2)	0.54751(3)	60.510(2)
$La_{0.70}Sr_{0.28}Mn_{0.99}O_3$	0.55058(2)	1.33547(4)	0.35059(4)	0.5470(1)	60.433(3)
$La_{0.90}Na_{0.09}Mn_{0.97}O_3$[a]	0.55267(1)	1.33510(3)	0.35316(3)	0.54760(1)	60.613(2)
$La_{0.90}K_{0.06}Mn_{0.99}O_3$[a]	0.55372(4)	1.33839(2)	0.35538(2)	0.54885(3)	60.588(2)
$La_{0.94}Rb_{0.06}Mn_{0.96}O_3$[a]	0.55406(1)	1.33969(2)	0.35616(2)	0.54931(1)	60.572(2)

[a] Quenched sample.

As α approaches 60.0° the lattice distortion vanishes. The remarkable effect of substitution bringing about the disappearance of the dissolution of lattice distortion is noteworthy. This effect becomes more pronounced as the ionic radii of the A ion becomes larger. The changes in a_h, c_h, V_h, and a_r with substitution are not monotonic. We cannot find out a simple rule which applies to all substitutions.

Comparing the furnace-cooled samples with the quenched samples having the same initial composition, all values for a_h, c_h, V_h, a_r, and α are larger for quenched samples than for furnace-cooled samples. The origin of these changes is thought to be due to the increase of the ionic radius of Mn, because the decrease of the lattice defect is hardly thought to arise from the lattice expansion. Similar decreases of unit cell volume with a decrease of defects were reported for layered calcium titanates (13).

Tables 3, 4, and 5 show the results of Rietveld analysis for $La_yNa_xMn_wO_3$ (x = 0, 0.09, and 0.16), $La_ySr_xMn_wO_3$, and $La_yRb_xMn_wO_3$, respectively, with the hexagonal setting. The refinement using the space group $R\bar{3}c$ yielded the smallest R factors. Figure 1 shows observed, calculated, and the difference of the X-ray diffraction pattern for $La_{0.95}Mn_{0.93}O_3$. The inset shows the result of the Rietveld refinement between 30° and 35° in 2θ. This type of splitting of the main peak indicates the rhombohedral distortion of lattice.

Figure 2a shows the relation between the Mn–O distance and a_{rhomb} and Fig. 2b shows the relation between α and the Mn–O–Mn angles. In the space group $R\bar{3}c$ the Mn–O distance is unique. A clear relation is seen between the Mn–O–Mn angles and α. The Mn–O–Mn angle becomes closer to 180° with an increase of x for A = Na. In the case of A = Sr, a slight increase of the Mn–O–Mn angle with x is seen. For A = Rb, the quenched samples ($La_{0.94}Rb_{0.06}Mn_{0.96}O_3$) have larger α and smaller Mn–O–Mn angles. The deviations of the O–Mn–O bond angle from 90° are small in all samples; the distortion of lattice is mainly reflected in the rotation angle of the octahedron.

Electrical Resistivity

The temperature dependence of resistivity for $La_{0.95}Mn_{0.93}O_3$ is shown in Fig. 3. $La_{0.95}Mn_{0.93}O_3$ shows a semiconducting temperature dependence of the resistivity. On the other hand, the temperature dependence of resistivities in alkali substituted samples is apparently different from that of $La_{0.95}Mn_{0.93}O_3$. Figures 4, 5, and 6 show the temperature dependence of resistivities for $La_yNa_xMn_wO_3$, $La_yA_xMn_wO_3$ (A = K and Rb), and $La_ySr_xMn_wO_3$, respectively. In the substituted samples, there is a transition from semiconductor to metal in the resistivity; below this transition temperature dependence of resistivity becomes metal-like.

Except for A = Na, the magnitude of resistivities and the transition temperature change monotonically with the increase of x. For A = K and Sr, the samples having the largest x shows the smallest absolute values of resistivities and the highest transition temperature.

The origin of this reduction of resistivities should be attributed to the systematic change in structure, because there is no systematic change in the valence state of Mn with alkali substitution. From spectroscopic studies (14), $LaMnO_{3.00}$ is reported to be the charge transfer type (CT) semiconductor. The energy gap reflects the energy difference between the empty upper-Hubbard band and filled O 2p band. The increase of Mn–O–Mn angles indicates an increase of band width; thus, the energy gap must decrease as the Mn–O–Mn angle increases and metallic conductivity appears when the energy gap disappears.

TABLE 3
Crystallographic Information for $La_yNa_xMn_wO_3$

	$La_{0.95}Mn_{0.93}O_3$	$La_{0.88}Na_{0.09}Mn_{0.96}O_3$	$La_{0.82}Na_{0.16}Mn_{1.00}O_3$
a(nm)	0.55266(1)	0.55142(1)	0.54903(1)
c(nm)	1.33345(1)	1.33347(1)	1.33186(2)
Occupation factor(G), atomic positions, and isotropic thermal parameters			
(La, Na)(6a)			
G	0.953	0.975	0.980
$B_{eq.}$(nm^2)	0.0080(7)	0.0076(7)	0.0047(6)
Mn(6b)			
G	0.935	0.955	1.00
$B_{eq.}$(nm^2)	0.002(1)	0.003(1)	0.001(1)
O(18e)			
x	0.551(3)	0.549(3)	0.546(3)
$B_{eq.}$(nm^2)	0.005(4)	0.010(4)	0.007(3)
Bond length(nm)			
La, Na–Mn (×8)	0.3379(1)	0.3372(1)	0.3359(1)
La, Na–O (×3)	0.248(1)	0.249(2)	0.249(1)
La, Na–O (×6)	0.2750(1)	0.2747(2)	0.2739(1)
La, Na–O (×3)	0.304(1)	0.303(2)	0.302(1)
Mn–O (×6)	0.1964(2)	0.1960(2)	0.1951(2)
O–O (×4)	0.2750(2)	0.2747(2)	0.2739(1)
O–O (×4)	0.2805(4)	0.2796(5)	0.2779(3)
Bond angle/degree			
Mn–O–Mn	163.7(8)	164.2(9)	165.2(7)
O–Mn–O	91.14(6)	91.02(6)	90.84(5)
O–Mn–O	88.86(6)	89.98(6)	89.16(5)
La, Na–O–La, Na	84.2(3)	84.4(4)	84.8(3)
La, Na–O–La, Na	168.4(6)	168.8(7)	169.5(5)
La, Na–O–Mn	81.8(4)	82.1(5)	82.6(4)
La, Na–O–Mn	88.37(8)	88.55(9)	88.81(7)
R values(%)			
R_{wp}	8.55	9.45	8.94
R_p	5.97	6.89	6.88
R_r	8.42	9.31	9.47
R_e	4.44	4.42	6.09
R_i	2.69	2.75	1.85
R_f	1.62	1.65	1.43
(Chisqr.)	(3.706)	(4.5765)	(2.1537)

Note. The three unique atoms in space group $R\bar{3}c$ have the following positions: Mn(0, 0, 0); (La, Na)(0, 0, 0.25); O(x, 0, 0.25).

There are two peaks in resistivity in $La_{0.88}Na_{0.09}Mn_{0.96}O_3$, $La_{0.87}K_{0.06}Mn_{0.97}O_3$, and $La_{0.91}Rb_{0.06}Mn_{0.94}O_3$ whose initial composition are $La_{0.9}A_{0.1}MnO_3$. These two peaks in resistivities suggest the possibility of coexistence of two phases, although from powder X-ray diffraction for these samples the existence of secondary phase was not confirmed. To confirm the existence of the secondary phase, quenching from 1393 K into liquid nitrogen was carried out for three samples of $La_{0.88}Na_{0.09}Mn_{0.96}O_3$, $La_{0.87}K_{0.06}Mn_{0.97}O_3$, and $La_{0.91}Rb_{0.06}Mn_{0.94}O_3$. If two peaks in resistivities are due to the phase separation, the change of valence state in Mn should be reflected in the temperature dependence of resistivities. The composition and valence state of Mn in quenched samples are listed in Table 1 for furnace-cooled samples. There is a certain decrease of valence state of Mn for quenched samples and thus w approaches unity. The lattice parameters and unit cell volume of quenched samples are listed in Table 2, and the results of the Rietveld

TABLE 4
Crystallographic Information for $La_ySr_xMn_wO_3$

	$La_{0.86}Sr_{0.09}Mn_{0.95}O_3$	$La_{0.78}Sr_{0.18}Mn_{0.97}O_3$	$La_{0.70}Sr_{0.28}Mn_{0.99}O_3$
a(nm)	0.55242(1)	0.55172(1)	0.55058(1)
c(nm)	1.33481(1)	1.33590(2)	1.33547(2)
Occupation factor(G), atomic positions, and isotropic thermal parameters			
(La, Sr)(6a)			
G	0.946	0.964	0.980
$B_{eq.}$(nm^2)	0.0054(7)	0.0043(7)	0.003(1)
Mn(6b)			
G	0.946	0.974	0.990
$B_{eq.}$(nm^2)	0.000(1)	0.000(1)	0.001(2)
O(18e)			
x	0.549(3)	0.545(2)	0.545(4)
$B_{eq.}$(nm^2)	0.005(4)	0.007(4)	0.005(6)
Bond length(nm)			
La, Sr–Mn (×8)	0.3378(1)	0.3374(1)	0.3368(1)
La, Sr–O (×3)	0.250(2)	0.251(1)	0.251(2)
La, Sr–O (×6)	0.2750(2)	0.2749(1)	0.2746(2)
La, Sr–O (×3)	0.302(2)	0.301(1)	0.300(2)
Mn–O (×6)	0.1962(2)	0.1959(2)	0.1956(3)
O–O (×4)	0.2750(2)	0.2749(2)	0.2746(2)
O–O (×4)	0.2799(5)	0.2792(2)	0.2786(7)
Bond angle(degree)			
Mn–O–Mn	165.3(10)	165.4(8)	165.5(13)
O–Mn–O	91.02(6)	90.90(5)	90.82(8)
O–Mn–O	88.91(6)	89.10(5)	89.18(5)
La, Sr–O–La, Sr	84.5(3)	84.8(3)	84.8(3)
La, Sr–O–La, Sr	169.0(7)	169.6(6)	169.7(9)
La, Sr–O–Mn	82.3(5)	82.7(4)	82.7(7)
La, Sr–O–Mn	88.54(9)	88.7(4)	88.8(1)
R values(%)			
R_{wp}	9.35	9.24	14.08
R_p	6.51	6.82	11.12
R_r	8.41	8.58	13.61
R_e	4.81	4.72	4.66
R_i	2.73	1.91	2.82
R_f	1.70	1.18	1.58
(Chisqr.)	(3.7753)	(3.8289)	(9.1293)

Note. The three unique atoms in space group $R\bar{3}c$ have the following positions: Mn(0, 0, 0); (La, Sr)(0, 0, 0.25); O(x, 0, 0.25).

refinement to $La_{0.91}Rb_{0.06}Mn_{0.94}O_3$ (furnace-cooled sample) and $La_{0.94}Rb_{0.06}Mn_{0.96}O_3$ (quenched sample) are summarized in Table 5. Quenched samples have larger lattice parameters and unit cell volumes. The α values are also larger in the quenched samples, thus, the rhombohedral distortion increases with quenching. Rietveld refinement for two Rb substituted samples using the space group $R\bar{3}c$ gave the smallest R factors: there is no change in lattice symmetry with quenching.

Figure 7 shows the temperature dependence of resistivities for $La_{0.88}Na_{0.09}Mn_{0.96}O_3$ (furnace cooled) and for $La_{0.90}Na_{0.09}Mn_{0.97}O_3$ (quenched) samples. The absolute value of resistivity increases after quenching but two peaks still remain. The resistivity of quenched $La_{0.90}K_{0.06}Mn_{0.99}O_3$ showed behavior similar to $La_{0.87}K_{0.06}Mn_{0.97}O_3$. The results in Na and K substituted systems suggest that there are no secondary phases in these systems. If there are secondary phases in these samples, the amount of secondary phase

TABLE 5
Crystallographic Information for $La_{0.91}Rb_{0.06}Mn_{0.94}O_3$ (Furnace-Cooled) and $La_{0.94}Rb_{0.06}Mn_{0.96}O_3$ (quenched)

	$La_{0.91}Rb_{0.06}Mn_{0.94}O_3$	$La_{0.94}Rb_{0.06}Mn_{0.96}O_3$
a(nm)	0.55270(1)	0.55406(1)
c(nm)	1.33385(2)	1.33969(2)
Occupation factor (G), atomic positions, and isotropic thermal parameters		
	(La, Rb)(6a)	
G	0.969	1.00
B/eq. (nm^2)	0.0063(7)	0.0053(7)
	Mn(6b)	
G	0.940	0.962
B/eq. (nm^2)	0.002(1)	0.001(1)
	O(18e)	
x	0.543(3)	0.547(3)
B/eq. (nm^2)	0.010(4)	0.010(3)
	Bond length (nm)	
La, Rb–Mn (×8)	0.3380(1)	0.3388(1)
La, Rb–O (×3)	0.252(2)	0.251(2)
La, Rb–O (×6)	0.2753(1)	0.2759(2)
La, Rb–O (×3)	0.301(2)	0.303(1)
Mn–O (×6)	0.1962(2)	0.1968(2)
O–O (×4)	0.2754(1)	0.2759(2)
O–O (×4)	0.2796(4)	0.2807(5)
	Bond angle (degree)	
Mn–O–Mn	165.7(9)	164.7(10)
O–Mn–O	90.87(5)	90.99(7)
O–Mn–O	89.13(5)	89.01(7)
La, Rb–O–La, Rb	84.9(3)	84.6(4)
La, Rb–O–La, Rb	169.8(6)	169.1(7)
La, Rb–O–Mn	82.9(5)	82.4(5)
La, Rb–O–Mn	88.76(8)	88.59(9)
	R values (%)	
R_{wp}	9.61	10.71
R_p	6.78	7.45
R_r	8.58	9.29
R_e	5.14	5.13
R_i	4.26	3.94
R_f	2.13	1.99
(Chisqr.)	(3.4988)	(4.3521)

Note. The three unique atoms in space group $R\bar{3}e$ have the following positions: Mn (0, 0, 0); (La, Rb) (0, 0, 0.25); O (x, 0, 0.25).

compared to that of main phase must change with quenching since the valence state of Mn clearly changes with substitution. In such a case, change in the profile of temperature dependence of resistivities, such as alternation of the relative height of the resistivity peaks, should appear with quenching. The experiment of quenching revealed that both two peaks are originating from the main phase.

Figure 8 shows the temperature dependence of resistivities for $La_{0.91}Rb_{0.06}Mn_{0.94}O_3$ (furnace cooled) and for $La_{0.94}Rb_{0.06}Mn_{0.96}O_3$ (quenched). In these Rb substituted systems there are clear changes with quenching in the profiles of the temperature dependence of resistivities: the peak at the lower temperature side disappears and temperature dependence of resistivity becomes semiconducting down to 10 K. Since the coexistence of secondary phase is hardly considered from the results of Na and K substituted samples, this change of resistivity is thought to be intrinsic. This semiconducting behavior may be due to the large Mn–O–Mn bond length which for $La_{0.94}Rb_{0.06}Mn_{0.96}O_3$ and $La_{0.95}Mn_{0.93}O_3$ are 0.1968(2) nm and 0.1964(2) nm, respectively; they are the two largest Mn–O–Mn bond lengths in the samples synthesized in this study. A more detailed analysis is needed about the behavior of resistivities of $La_{0.95}Mn_{0.93}O_3$ and $La_{0.94}Rb_{0.06}Mn_{0.96}O_3$, because these two samples also show a ferromagnetic transition at lower temperature as ascribed below.

Magnetic Susceptibility

Figures 9, 10, and 11 show the reciprocal magnetic susceptibilities for $La_{0.95}Mn_{0.93}O_3$, $La_yNa_xMn_wO_3$, $La_yA_xMn_wO_3$ (A = K and Rb), and $La_ySr_xMn_wO_3$, respectively. All samples including $La_{0.95}Mn_{0.93}O_3$ exhibit a ferromagnetic transition. The transition temperature T_c, paramagnetic Curie temperature Θ, and Curie constant C are summarized in Table 6. Θ was determined from the least square fit of susceptibilities to Curie–Weiss law,

$$\chi = C/(T - \Theta), \qquad [1]$$

between 500 and 700 K. T_c, defined as the temperature at which extrapolated reciprocal susceptibilities vanishes, was determined from the extrapolation of reciprocal susceptibility to the low temperature region. T_c determined in this manner is in a good agreement with the transition determined by the SQUID at low temperature for samples having transition temperature lower than 300 K. Thus, the transition temperature determined by the extrapolation can be regarded as accurate even for T_c higher than 300 K. T_c increases monotonically as x increases, except for $x = 0.16$ with A = Na. Θ also increases as x increases; Θ values are about 40–80 K higher than T_c, except for three samples. The samples in which Θ is equal to T_c are $La_{0.84}Na_{0.12}Mn_{0.99}O_3$, $La_{0.82}K_{0.14}Mn_{1.02}MnO_3$, and $La_{0.70}Sr_{0.28}Mn_{0.99}O_3$. It is apparent that all samples show a ferromagnetic transition.

The Curie temperature of ferromagnet are given by the well known formula

$$T_c = 2zJS(S + 1)/3k_B, \qquad [2]$$

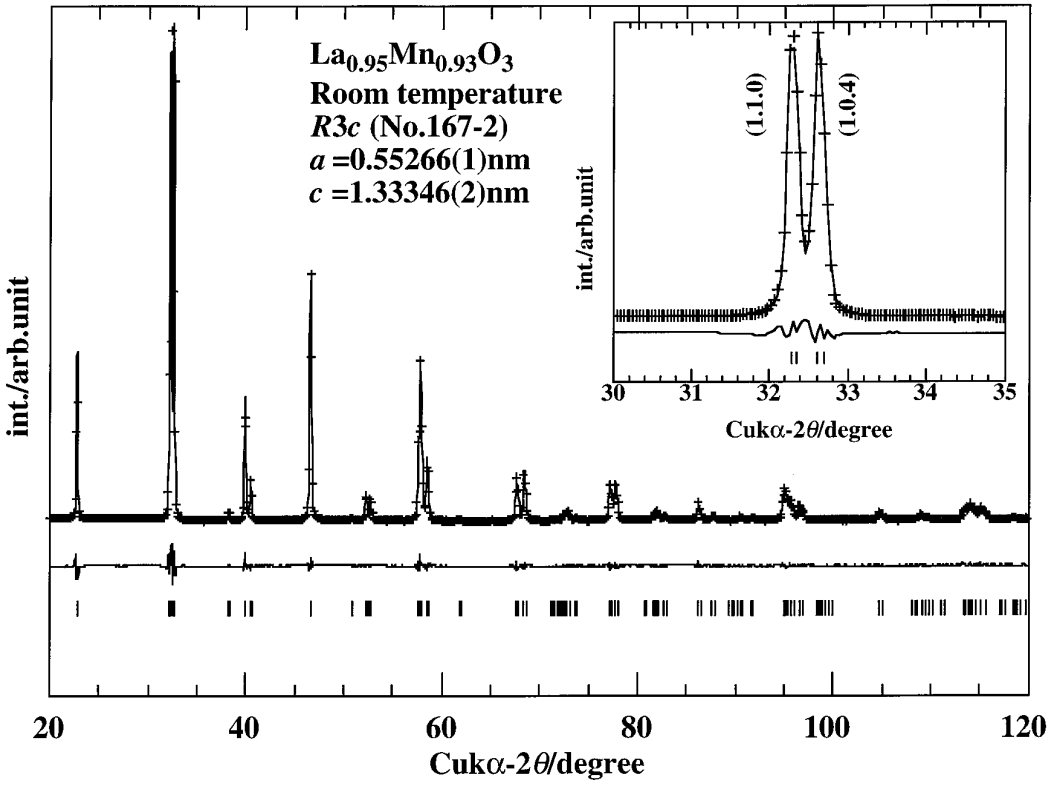

FIG. 1. Plot of observed (+) and calculated intensities, peak positions (I) of $La_{0.95}Mn_{0.93}O_3$. Calculation was carried out supposing space group $R\bar{3}c$. The residuals appears below the intensities.

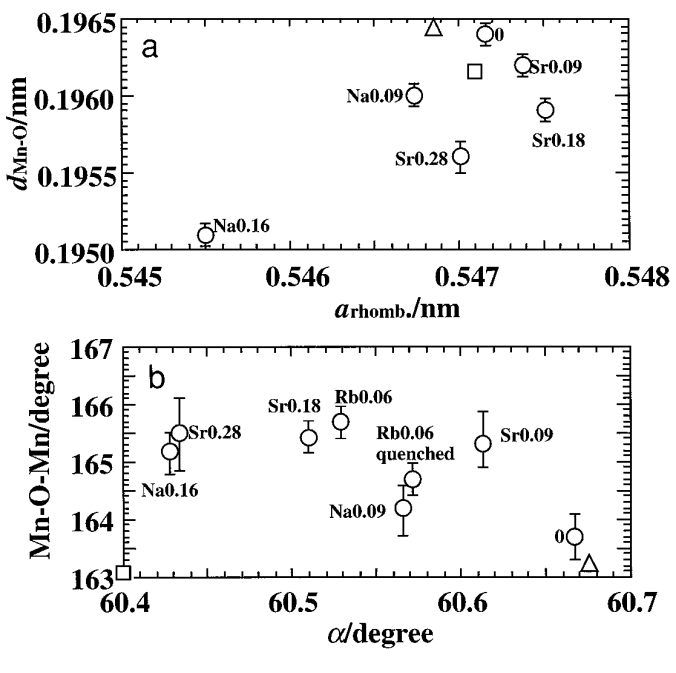

FIG. 2. (a) The $a_{rhomb.}$ dependence of Mn–O distance. (b) The α dependence of Mn–O–Mn angles. Squares are the data for $LaMnO_{3.12}$ (10) and triangles are for $LaMnO_{3.158}$ (11).

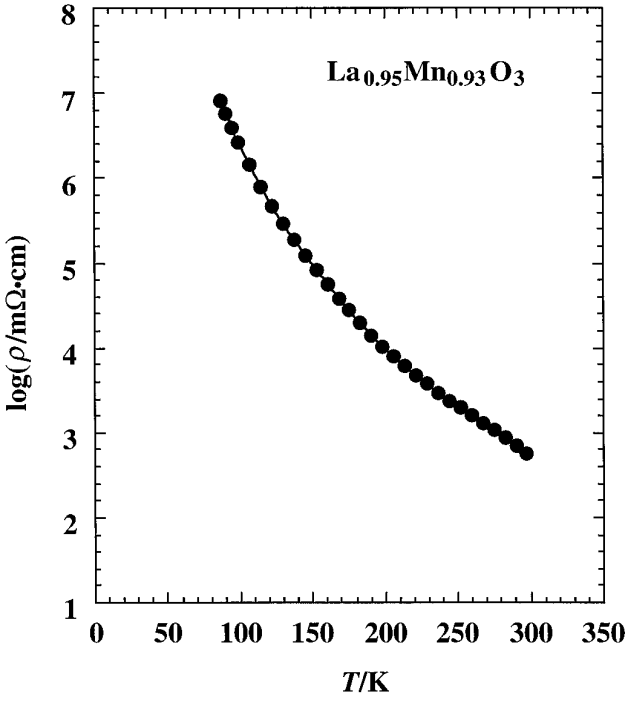

FIG. 3. Temperature dependence of logarithm electrical resistivity for $La_{0.95}Mn_{0.93}O_3$.

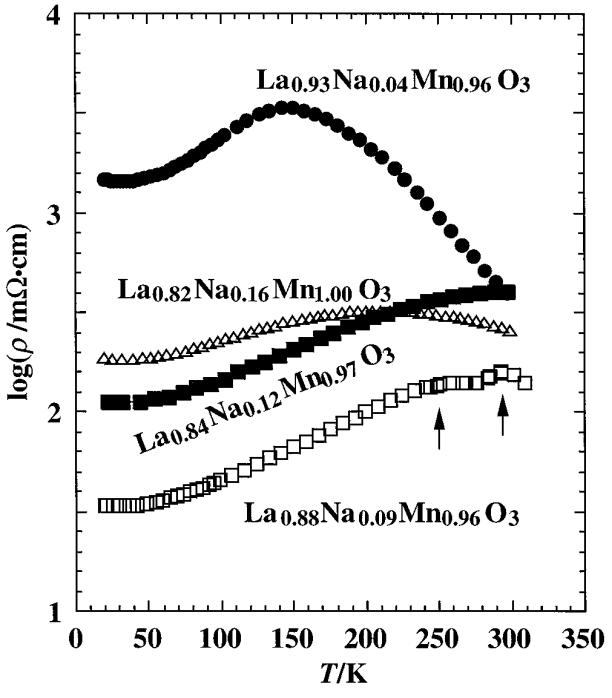

FIG. 4. Temperature dependence of electrical resistivities for $La_xNa_yMn_wO_3$. ↑ indicates the peak or hump in resistivity.

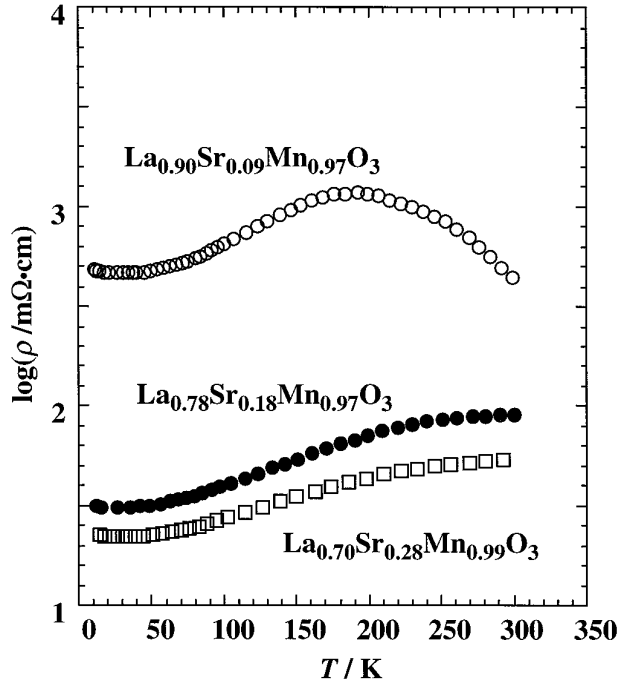

FIG. 6. Temperature dependence of electrical resistivities for $La_xSr_yMn_wO_3$.

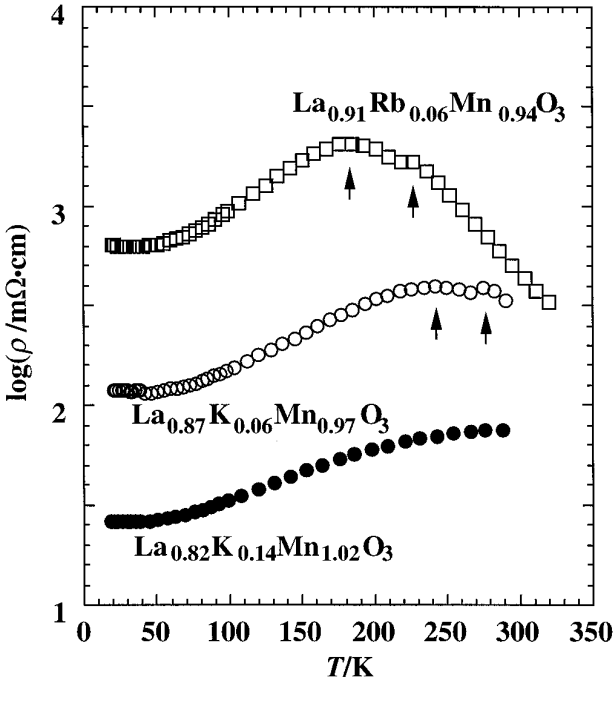

FIG. 5. Temperature dependence of electrical resistivities for $La_xNa_yMn_wO_3$ (A = K and Rb).

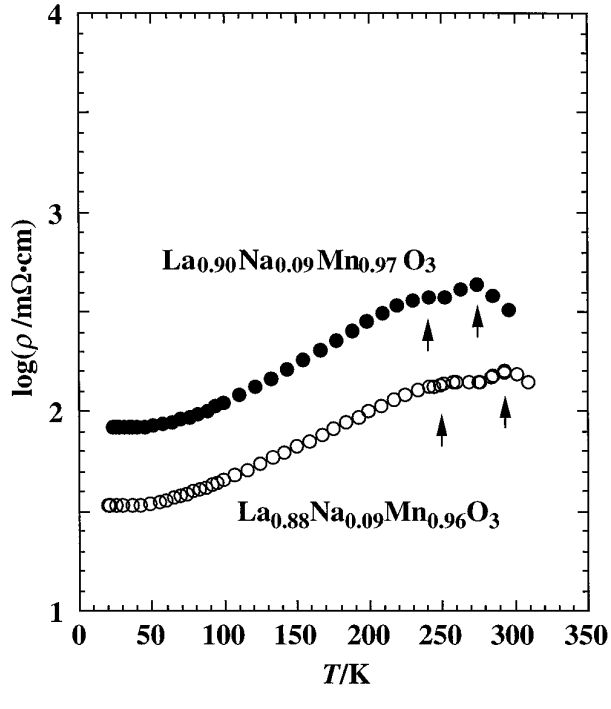

FIG. 7. Temperature dependence of electrical resistivities for $La_{0.88}Na_{0.09}Mn_{0.96}O_3$ (furnace-cooled) and $La_{0.90}Na_{0.09}Mn_{0.97}O_3$ (quenched).

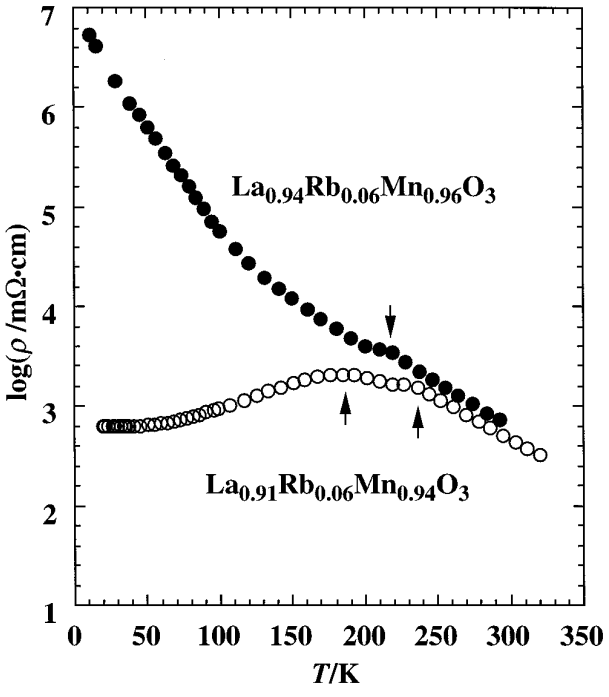

FIG. 8. Temperature dependence of electrical resistivities for $La_{0.91}Rb_{0.06}Mn_{0.94}O_3$ (furnace-cooled) and $La_{0.94}Rb_{0.06}Mn_{0.96}O_3$ (quenched).

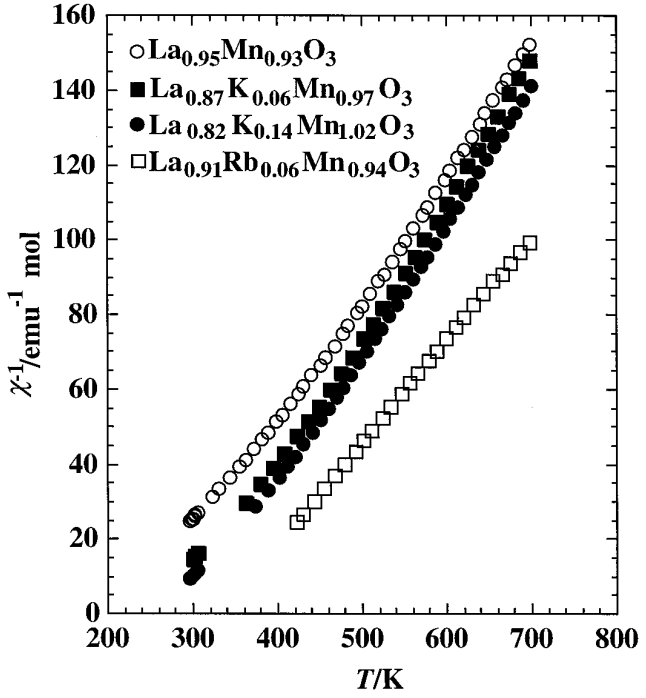

FIG. 10. Temperature dependence of inverse of molar magnetic susceptibilities for $La_xA_yMn_wO_3$ (A = K and Rb).

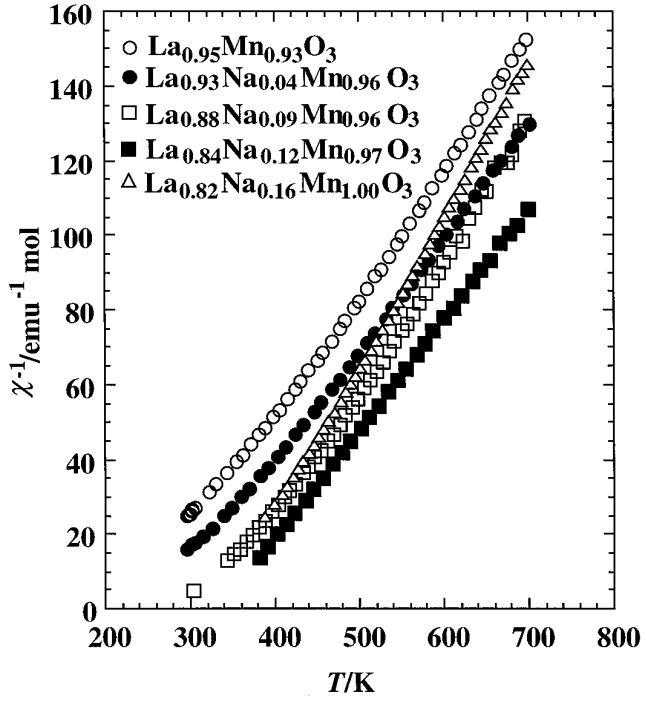

FIG. 9. Temperature dependence of inverse molar magnetic susceptibilities for $La_xNa_yMn_wO_3$.

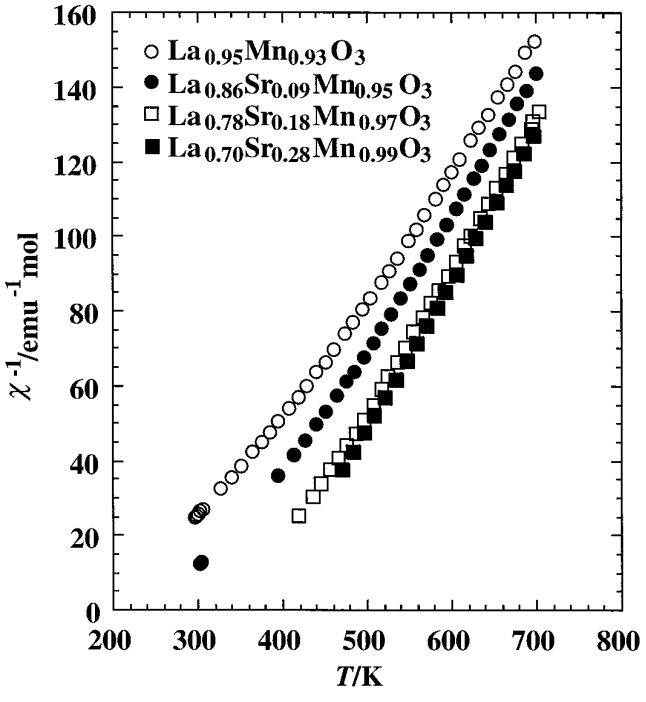

FIG. 11. Temperature dependence of inverse of molar magnetic susceptibilities for $La_xSr_yMn_wO_3$.

TABLE 6
C, Θ, T_c, and $\Theta - T_c$ for $La_yA_xMn_wO_3$

Composition	C(emu · K · mol^{-1})	Θ(K)	T_c(K)	$\Theta - T_c$(K)
$La_{0.95}Mn_{0.93}O_3$	2.74	279	185	94
$La_{0.93}Na_{0.04}Mn_{0.96}O_3$	2.98	281	219	62
$La_{0.88}Na_{0.09}Mn_{0.96}O_3$	2.56	363	286	77
$La_{0.84}Na_{0.12}Mn_{0.97}O_3$	2.99	336	336	0
$La_{0.82}Na_{0.16}Mn_{1.00}O_3$	2.38	352	308	42
$La_{0.87}K_{0.06}Mn_{0.97}O_3$	2.73	316	270	46
$La_{0.82}K_{0.14}Mn_{1.02}O_3$	2.86	330	330	0
$La_{0.91}Rb_{0.06}Mn_{0.94}O_3$	2.58	316	234	82
$La_{0.86}Sr_{0.09}Mn_{0.95}O_3$	2.58	328	246	72
$La_{0.78}Sr_{0.18}Mn_{0.97}O_3$	2.49	372	326	46
$La_{0.70}Sr_{0.28}Mn_{0.99}O_3$	2.53	376	376	0
$La_{0.90}Na_{0.09}Mn_{0.97}O_3$	2.93	340	274	66
$La_{0.90}K_{0.06}Mn_{0.99}O_3$[a]			260	
$La_{0.94}Rb_{0.06}Mn_{0.96}O_3$[a]			222	

[a] For these samples only SQUID measurement below 300 K was carried out.

where z, J, and S are the numbers of nearest magnetic neighbors, the strength of magnetic interaction, and the size of spin momentum, respectively. The increases in T_c and Θ with x are not due to the increase of J with the increase of Mn^{4+} population because there is no systematic increase of the valence state of Mn with the substitution. The reason for this increase must come from the structural change. We have measured the saturation magnetization down to 5 K for some samples. Saturation moments, n_B, for $La_{0.95}Mn_{0.93}O_3$, $La_{0.93}Na_{0.04}Mn_{0.96}O_3$, $La_{0.88}Na_{0.09}Mn_{0.96}O_3$, $La_{0.84}Na_{0.12}Mn_{0.97}O_3$, $La_{0.82}Na_{0.16}Mn_{1.00}O_3$, $La_{0.82}K_{0.14}Mn_{1.02}O_3$, and $La_{0.91}Rb_{0.06}Mn_{0.94}O_3$ are 3.19, 3.67, 3.64, 3.76, 3.46, 3.42, and 3.74, respectively. Figure 12 shows the relation between T_c and the valence state of Mn of $La_yA_xMn_wO_3$. There is no clear relation between T_c and the valence of Mn. For example, T_c of $La_{0.95}Mn_{0.93}O_3$ is 185 K, the lowest value in this $La_yA_xMn_wO_3$ system, but the valence 3.36(3) is not the lowest in the $La_yA_xMn_wO_3$ system. Similarly, the valence 3.37(3) for $La_{0.70}Sr_{0.28}Mn_{0.99}O_3$ is also not the highest value in the $La_yA_xMn_wO_3$ system. Moreover, in comparing the T_c of three furnace-cooled samples and three quenched samples having the same initial compositions, the T_c of quenched samples are lower by only about 10 or 20 K. As shown in Table 1, the valence of quenched samples are always smaller than the furnace cooled samples by at least 0.11. These results suggest that the valence state of Mn plays a minor role in the increase of T_c and Θ. As shown in Table 1, w increases with x. Since z is equal to $6w$ except for $La_{0.82}K_{0.14}Mn_{1.02}O_3$, z increases with substitution. The smallest z is 5.58 in $La_{0.95}Mn_{0.93}O_3$ and the largest z is 6.00 in $La_{0.80}Na_{0.16}Mn_{1.00}O_3$. Thus, the increase in z contributes to the increase of T_c or Θ with substitution, although this increase of z is too small to explain the entire increase of T_c or Θ. In $La_yA_xMn_wO_3$, four types of magnetic interactions are considered. They are the Mn^{4+}–O^{2-}–Mn^{4+} superexchange interaction, the Mn^{3+}–O^{2-}–Mn^{3+} superexchange interaction, the Mn^{3+}–O^{2-}–Mn^{4+} superexchange interaction, and the Mn^{3+}–O^{2-}–Mn^{4+} double exchange. The dominant interaction between Mn^{3+}–O^{2-}–Mn^{4+} seems to be the double exchange interaction. Since the superexchange interaction does not accompany the transfer of conductive carriers even when the

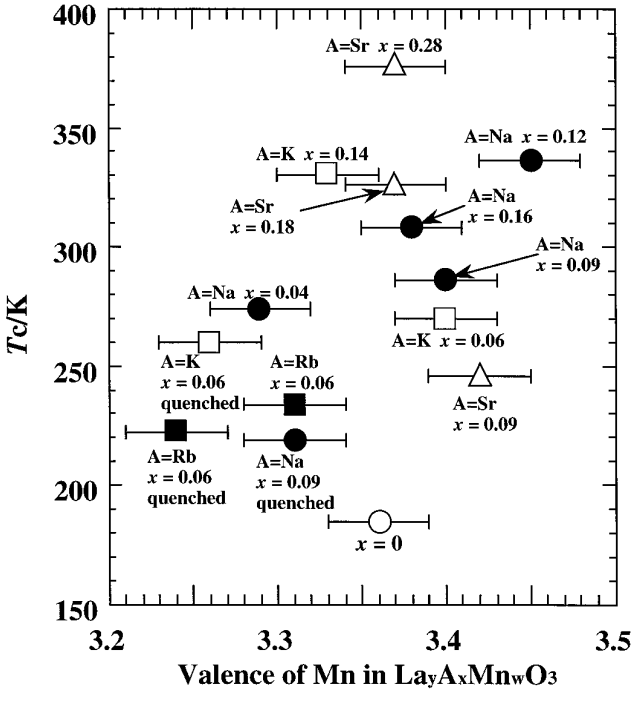

FIG. 12. Magnetic transition temperature expressed as a function of valence state of Mn in $La_yA_xMn_wO_3$.

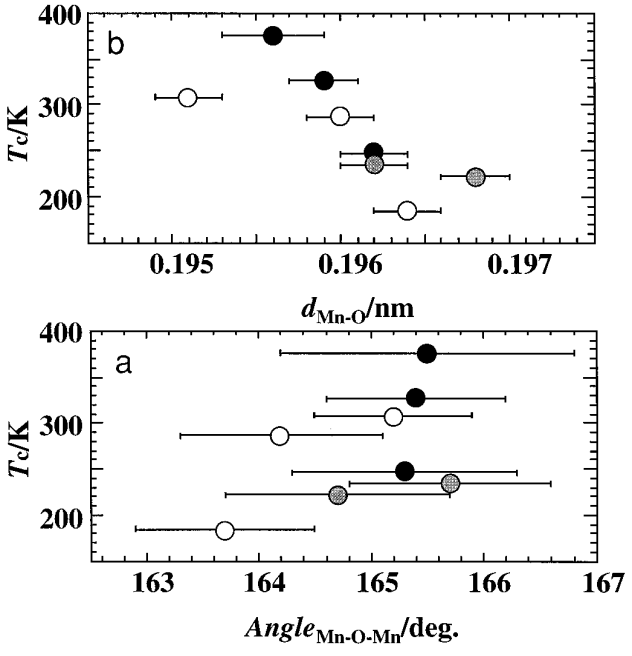

FIG. 13. Magnetic transition temperature expressed as a function of (a) Mn–O–Mn angles or (b) Mn–O distance in $La_yA_xMn_wO_3$. Open circles are the data for A = Na or x = 0, closed circles are for A = Sr, and hatched circles are for A = Rb.

Mn^{3+}–O^{2-}–Mn^{4+} interaction dominates no metallic conduction should be obtained. The large difference between T_c and Θ also suggests the existence of double exchange interactions. This difference may come from the strengthening of the magnetic interaction in the paramagnetic high temperature region. The possible reason for this strengthening is increase of conductivity with the increase of carrier concentration by thermal activation in the semiconducting region. For Mn^{4+}–O^{2-}–Mn^{4+} bonding, only weak antiferromagnetic interaction is predicted (15). Since the average valence of Mn is always lower than 3.5 the antiferromagnetic Mn^{4+}–O^{2-}–Mn^{4+} interaction is thought to be unimportant. The antiferromagnetic transitions is really not observed in this study. On the other hand, the Mn^{3+}–O^{2-}–Mn^{3+} superexchange interaction is important (15). It is relatively strong compared to Mn^{4+}–O^{2-}–Mn^{4+} interaction, and it becomes both ferromagnetic or antiferromagnetic, along with the change in bond distance and bond angle. In particular, the magnetic structure of antiferromagnetic $LaMnO_3$ is so-called A-type, which leads to ferromagnetic order of nearest neighbor of Mn. If the Mn^{3+}–O^{2-}–Mn^{3+} superexchange were only antiferromagnetic, the magnetic structure of $LaMnO_3$ should become G-type like $LaFeO_3$ and $LaCoO_3$. Previous reports by Havinga (16) and Watanabe (17) showed that the sign of the Mn^{3+}–O^{2-}–Mn^{3+} superexchange interaction becomes negative (= antiferromagnetic) when the Mn^{3+}–O^{2-} distance is short and the deviation of the Mn^{3+}–O^{2-}–Mn^{3+} angle from 180° is large, as predicted by Goodenough (15). According to their reports, in $La_yA_xMn_wO_3$ the Mn–O bond length and the Mn–O–Mn angle determined by Rietveld analysis always remain in the ferromagnetic range of the Mn^{3+}–O^{2-}–Mn^{3+} superexchange. Figures 13a and 13b show the plot of T_c as a function of the Mn–O bond length and also as a function of the Mn–O–Mn angle. Apparently, there is a significant dependence in T_c on structure. As the Mn–O distance decreases or Mn–O–Mn angle increases T_c sharply increases. However, the previously reported bond distance and angle dependence of the superexchange interaction strength is relatively small in the ferromagnetic region (16). For example, when the Mn–O–Mn bond angle increases from 160° to 180° the T_c increase should be only 20% (16, 17). According to these reports, T_c changes very slightly with the changes of Mn–O bond distance and Mn–O–Mn bond angle in the region exhibited in Figs. 13a and 13b. These results mean that the increase of T_c or Θ in $La_yA_xMn_wO_3$ is not due to the Mn^{3+}–O^{2-}–Mn^{3+} ferromagnetic superexchange. Figure 14 shows the relation between α and T_c in all $La_yA_xMn_wO_3$ compounds. Certainly, there is a clear increase of T_c with a decrease in α. As a result, the increase of T_c and Θ must originate from the structural dependence of the strength of the Mn^{3+}–O^{2-}–Mn^{4+} double exchange interaction. The reduction of rhombohedral distortion of lattice and resistivity with substitution also sup-

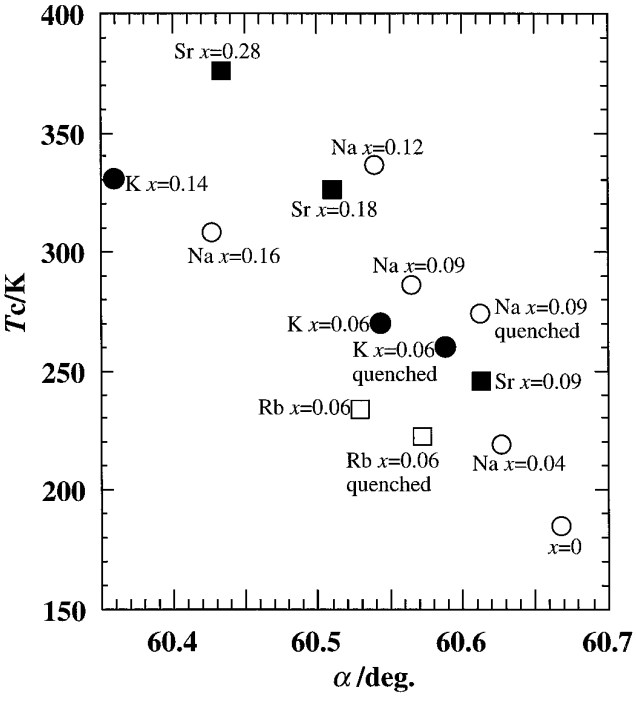

FIG. 14. Magnetic transition temperature expressed as a function of α in $La_yA_xMn_wO_3$.

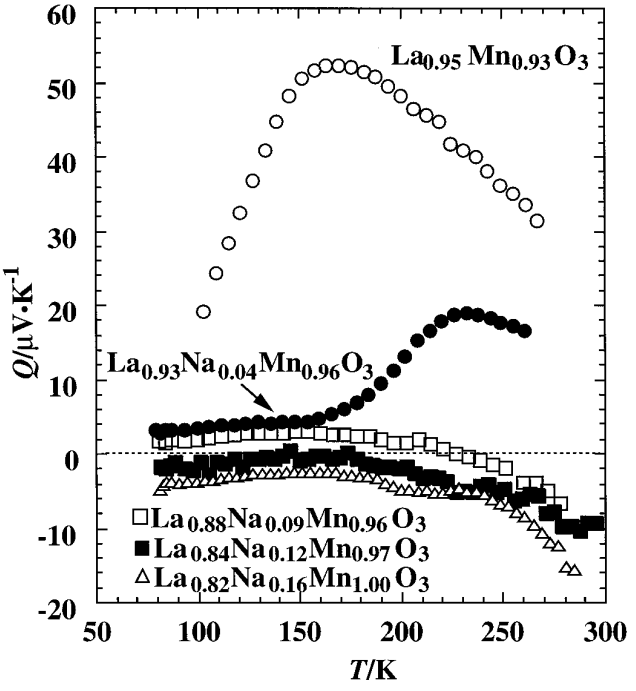

FIG. 15. Temperature dependence of Seebeck coefficients for $La_yNa_xMn_wO_3$.

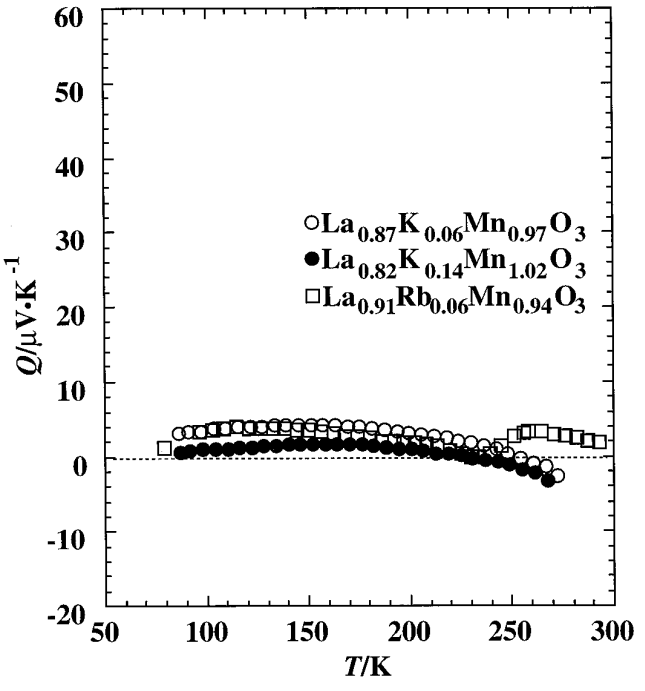

FIG. 16. Temperature dependence of Seebeck coefficients for $La_yA_xMn_wO_3$ (A = K and Rb).

port this result, although the semiconducting–metallic transition temperature in resistivities do not always coincide with T_c. Only in six samples, $La_{0.88}Na_{0.09}Mn_{0.96}O_3$, $La_{0.87}Na_{0.06}Mn_{0.97}O_3$, $La_{0.91}aRb_{0.06}Mn_{0.94}O_3$, $La_{0.90}Na_{0.09}Mn_{0.97}O_3$, $La_{090}K_{0.06}Mn_{0.99}O_3$, and $La_{0.94}Rb_{0.06}Mn_{0.96}O_3$ which have initial composition $La_{0.9}A_{0.1}MnO_3$ (A = Na, K, and Rb), does T_c agree with the peak temperatures in resistivity; in other samples T_c is higher.

Seebeck Coefficient

As shown above, T_c determined by extrapolations of the magnetic susceptibility is apparently higher than the temperatures at which some samples show the resistivity peak. For example, $La_{0.95}Mn_{0.93}MnO_3$ does not exhibit the semiconducting–metal transition in resistivity measurement but shows semiconducting behavior in resistivity down to 10 K, even though below 150 K ferromagnetism appears.

Even when the temperature for the peaks in resistivities is lower than T_c, the existence of a double exchange interaction is not in doubt, as judged by the results of Seebeck coefficient measurements. Figures 15, 16, and 17 show the temperature dependence of the Seebeck coefficient for $La_yNa_xMn_wO_3$, $La_yA_xMn_wO_3$ (A = K and Rb), and $La_ySr_xMn_wO_3$, respectively. A clear anomaly in the Seebeck coefficient is noted at T_c for the samples which have T_c below 270 K. This anomaly suggests that there is a certain change

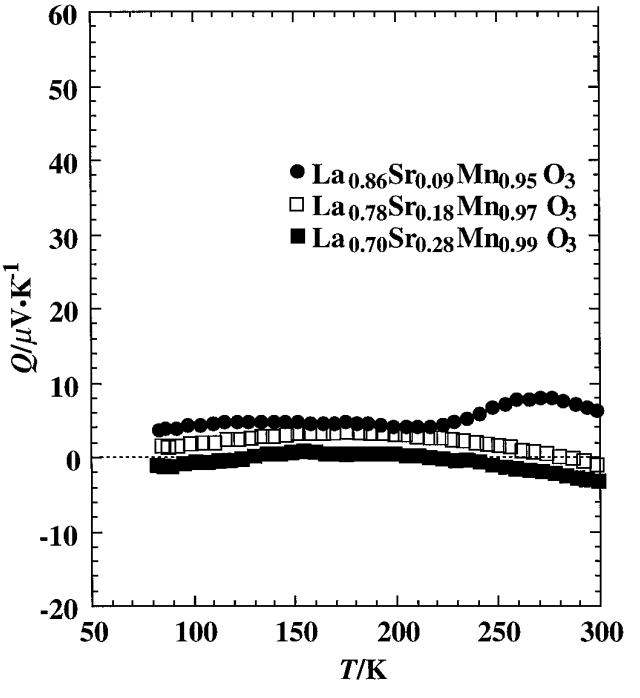

FIG. 17. Temperature dependence of Seebeck coefficients for $La_ySr_xMn_wO_3$.

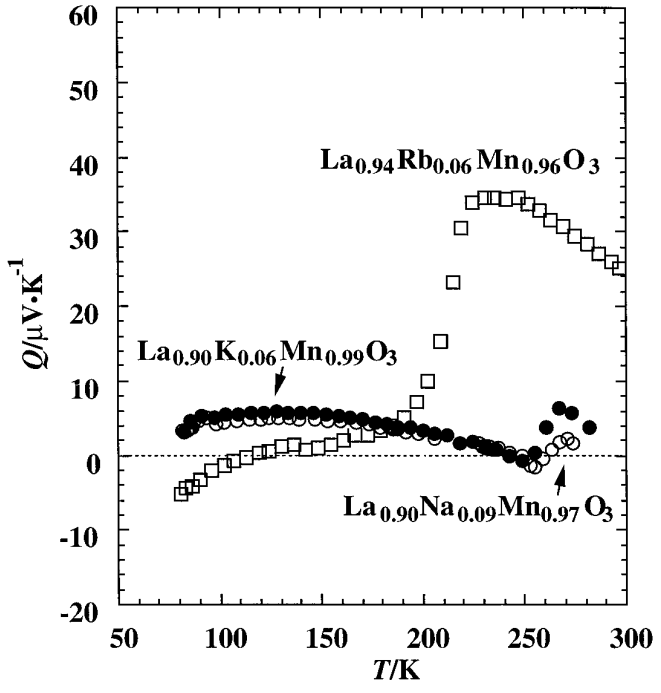

FIG. 18. Temperature dependence of Seebeck coefficients for quenched $La_{0.90}Na_{0.09}Mn_{0.97}O_3$, $La_{0.90}K_{0.06}Mn_{0.99}O_3$, and $La_{0.94}Rb_{0.06}Mn_{0.96}O_3$.

in band structure of these samples at T_c. The temperature dependence of Seebeck coefficients of three quenched samples, $La_{0.90}Na_{0.09}Mn_{0.97}O_3$, $La_{0.90}K_{0.06}Mn_{0.99}O_3$, and $La_{0.94}Rb_{0.06}Mn_{0.96}O_3$, are also shown in Fig. 18. The anomalies in the Seebeck coefficient appear at the temperature T_c which is also the temperature where the peak appears in resistivity. Even in $La_{0.95}Mn_{0.93}O_3$ and $La_{0.94}Rb_{0.06}Mn_{0.96}O_3$, showing the semiconducting behavior down to 10 K, the temperature dependence of Seebeck coefficients is not remarkably different from the samples which exhibit metallic conduction at low temperature. In particular, the temperature dependence of the Seebeck coefficient of $La_{0.94}Rb_{0.06}Mn_{0.96}O_3$ (quenched sample) is very similar to that of $La_{0.91}Rb_{0.06}Mn_{0.95}O_3$ (furnace-cooled sample), showing that $La_{0.94}Rb_{0.06}Mn_{0.96}O_3$ (quenched) is not a gap-type semiconductor. For a gap-type semiconductor a negative temperature dependence of Seebeck coefficient ($d|Q| \propto T^{-1}$) is predicted. A similar temperature dependence of Seebeck coefficient was reported by Tanaka *et al.* for $La_{0.8}Ca_{0.2}MnO_3$ (18). In our case, however, the behavior above T_c is apparently different. In their report the temperature dependence above T_c is that of a typical semiconductor, as indicated by the T^{-1} dependence of the Seebeck coefficient above T_c. But in the case of $La_yA_xMn_wO_3$, the Seebeck coefficient above T_c shows a linear dependence on temperature, as clearly seen in $La_{0.95}Mn_{0.93}O_3$, $La_{0.91}Rb_{0.06}Mn_{0.94}O_3$, and $La_{0.94}Rb_{0.06}Mn_{0.96}O_3$. As shown in Figs. 15 to 18, the Seebeck coefficient at the low temperature region is almost constant, and at temperatures about 30 K higher than T_c it increases sharply. This result suggests that the change of electronic state starts at this temperature, although there are no anomalies at this temperature in resistivity. A clear systematic decrease of Seebeck coefficient with substitution is recognized. Since the statistical error of the apparatus is less than 1 μVK^{-1}, it is certain that the sign of Seebeck coefficient changes from positive to negative as the degree of substitution increases. Since this change is not attributed to the increase of the valence state of Mn, this change cannot be due to the change of band filling. The possible reason for this change is the change in the band structure with substitution. The hole concentration measurement for $Sr_{1-x}La_xTiO_3$ suggests that the sign of mobile carriers in that system is always negative between $0 \leq x \leq 1$ (19). This means that when the conduction band has a *d* orbital character the sign of the Seebeck coefficient becomes negative. On the other hand, in the CT-type insulator, the conduction band has the character of the oxygen 2*p* orbital and the sign of mobile carrier could become either positive or negative. The change of the sign in the Seebeck coefficient in $La_yA_xMn_wO_3$ with substitution, therefore, seems to suggest a change from a CT-type conductor to the Mott-type conductor with substitution. The reduction of lattice distortion decreases the energy difference between lower and upper Hubbard bands. If the oxygen 2*p* band locates between the upper and lower Hubbard bands in $La_yA_xMn_wO_3$, the decrease of Hubbard splitting may result in an overlap of the oxygen 2*p* band and the Hubbard band. This change of band structure at the Fermi surface may be the cause for the change of the sign of Seebeck coefficient. The mixed (CT and Mott) character of $LaMnO_3$ due to comparable U_{dd} and Δ_{CT} values makes the interpretation of the obtained result fairly complicated.

CONCLUSIONS

The alkali metal or Sr substitution for La in $LaMnO_3$ does not result in a systematic variation of valency of manganese ions when the sample was fired at 1393 K in an oxygen gas flow. By the substitution, the semiconducting behavior of resistivity for $La_{0.95}Mn_{0.93}O_3$ changed to metallic behavior, except for the quenched Rb-substituted sample. All the samples were found to exhibit a ferromagnetic transition at low temperatures. The ferromagnetic transition temperature was found to be correlated with the degree of substitution but not with the valence state of manganese ions. A close relation seems to exist between the changes of electrical and magnetic properties and structure, especially the bond angle of Mn–O–Mn and bond distance Mn–O. These results imply a strong Mn^{3+}–O^{2-}–Mn^{4+} angle dependence of the double exchange interac-

tion. The semiconducting–metallic transition temperature was lower than the magnetic transition temperature but the reason cannot be clarified because polycrystalline samples were used. The anomalies in the Seebeck coefficient at the magnetic transition temperature also support the existence of the double exchange interaction.

ACKNOWLEDGMENT

Part of this work was supported by the Grant-in Aid for Scientific Research from Ministry of Education, Science, and Culture.

REFERENCES

1. G. H. Jonker and J. H. VanSanten, *Physica* **16,** 337 (1950).
2. G. H. Jonker, *Physica* **22,** 707 (1956).
3. C. Zenner, *Phys. Rev.* **83,** 299 (1951).
4. M. Verelst, N. Rangavittal, C. N. R. Rao, and A. Rousset, *J. Solid State Chem.* **74,** 104 (1993).
5. R. von Helmolt, J. Wecker, B. Holzapfel, L. Schultz, and K. Samwer, *Phys. Rev. Lett.* **71,** 2332 (1993).
6. M. Mccormack, S. Jin, T. H. Fleming, J. M. Phillips, and R. Ramesh, *Appl. Phys. Lett.* **64,** 3045 (1994).
7. R. Mahesh, R. Mahendiran, A. K. Raychaudhury, and C. N. R. Rao, *J. Solid State Chem.* **114,** 297 (1995).
8. F. Izumi, *J. Crystallogr. Soc. Jpn.* **27,** 2327 (1985).
9. R. J. H. Voorhoeve, J. P. Remeike, and D. W. Jhonson, Jr., *Science* **180,** 62 (1973).
10. B. C. Tofield and W. R. Scott, *J. Solid State Chem.* **10,** 183 (1974).
11. J. A. M. Van Roosmalen, E. H. O. Cordfunke, and R. B. Helmholdt, *J. Solid State Chem.* **110,** 100 (1994).
12. Y. Takeda, S. Nakai, T. Kojima, R. Kanno, N. Imanishi, G. Q. Shen, O. Yamamoto, M. Mori, C. Asakawa, and T. Abe, *Mater. Res. Bull.* **26,** 153 (1991).
13. I. S. Kim, M. Itoh, and T. Nakamura, *J. Solid State Chem.* **101,** 77 (1992).
14. T. Arima, Y. Tokura, and J. B. Torrance, *Phys. Rev. B* **48,** 17006 (1993).
15. J. B. Goodenough, ''Magnetism and the Chemical Bond.'' Interscience, New York, 1963.
16. E. E. Havinga, *Philips Res. Rept.* **21,** 432 (1961).
17. H. Watanabe, *J. Phys. Soc. Jpn.* **16,** 433 (1961).
18. J. Tanaka, M. Umehara, S. Tsukioka, and S. Ehara, *J Phys. Soc. Jpn.* **51,** 1236 (1982).
19. Y. Tokura, Y. Taguchi, Y. Okada, Y. Fujimori, T. Arima, Y. Kumagai, and Y. Iye, *Phys. Rev. Lett.* **70,** 2126 (1993).